Discrete Scale Invariance in Inflation: Log-periodic Modulations in the Primordial Spectrum

Jonathan Athanasio Rosa
Independent Research
(Dated: August 28, 2025)

The Λ Cold Dark Matter (ΛCDM) cosmological model has emerged as the standard framework for modern cosmology. It successfully accounts for the large-scale structure of the Universe, the cosmic microwave background (CMB) anisotropies, and the late-time accelerated expansion. Within this paradigm, a period of accelerated expansion—inflation—in the very early Universe provides the seeds for primordial perturbations that subsequently evolve into the structures observed today. Despite its empirical success, the microphysical origin of inflation remains unknown, and the inflationary sector is typically modeled by simple scalar-field potentials.

I. INTRODUCTION

The Λ Cold Dark Matter (ΛCDM) cosmological model has emerged as the standard framework for modern cosmology. It successfully accounts for the large-scale structure of the Universe, the cosmic microwave background (CMB) anisotropies, and the late-time accelerated expansion. Within this paradigm, a period of accelerated expansion—inflation—in the very early Universe provides the seeds for primordial perturbations that subsequently evolve into the structures observed today [1]. Despite its empirical success, the microphysical origin of inflation remains unknown, and the inflationary sector is typically modeled by simple scalar-field potentials.

A central feature of inflationary cosmology is the generation of an approximately scale-invariant spectrum of curvature perturbations. However, a wide variety of inflationary models predict deviations from exact scale invariance, often in the form of oscillatory "features" in the primordial power spectrum. These features arise from different physical mechanisms:

- **Axion monodromy inflation:** Periodic modulations induced by non-perturbative axion physics produce resonant oscillations in the power spectrum, with characteristic frequencies determined by axion couplings and monodromy scales [2].
- **Step-feature models:** A sudden change in the inflaton potential or its derivatives generates localized oscillations in the spectrum, often with sharp transients [3].
- **Resonant and trapped inflation:** Repeated particle production events or oscillatory couplings can also leave log-periodic imprints in $\mathcal{P}_{\mathcal{R}}(k)$ [4].

While these mechanisms differ in microphysics, they share the prediction of oscillatory signatures. The challenge lies in distinguishing their origin and assessing their statistical significance given current observational data. In particular, Planck 2018 constraints have placed stringent bounds on oscillatory models, limiting the amplitude of permissible modulations to the percent level or below.

A. Motivation from Discrete Scale Invariance

Discrete Scale Invariance (DSI) is a symmetry principle in which a system is invariant under rescaling by specific discrete factors rather than continuous dilations. This symmetry generically leads to log-periodic modulations in physical observables [5]. In statistical physics, DSI emerges in systems with hierarchical or fractal structures, and it has been argued that similar principles could operate in the primordial Universe [6]. If the inflaton potential exhibits approximate DSI, the resulting curvature spectrum would contain log-periodic oscillations with a single fundamental log-frequency.

The advantage of the DSI perspective is twofold:

1. **Economy of assumptions:** Unlike models that require special events (e.g. steps) or additional particle content, DSI inflation introduces only a single modulation characterized by amplitude A and frequency ω.
2. **Predictive falsifiability:** The log-periodic structure enforces a deterministic relation between the oscillation frequency in field space and the observed modulation in $\ln k$. This provides a clear observational target, making the hypothesis testable with both current and next-generation CMB and large-scale structure surveys.

B. Objectives of this Work

The goal of this paper is to perform a comprehensive, conservative, and falsifiable study of inflation with a log-periodically modulated quadratic potential. Our approach differs from earlier heuristic treatments in three respects:

- We provide detailed analytical derivations connecting the potential $V(\Phi)$ to the predicted form of $\mathcal{P}_{\mathcal{R}}(k)$, highlighting the scale dependence of the oscillatory frequency $\omega_{\rm eff}$.
- We perform numerical integrations of the background equations with high precision, extracting

the modulation period and amplitude from the horizon-exit spectrum. We find that the modulation is subtle, with average amplitude $\langle A_{\rm osc}\rangle \sim 0.16\%$, increasing to 1–5% near the end of inflation.

- We outline a statistical framework to confront the model with data, describing how MCMC analyses with Planck 2018 and upcoming CMB-S4/Euclid/SKA surveys can test the hypothesis decisively.

Our philosophy is humility: we do not claim to have found large, spectacular signals. Rather, we aim to present a theoretically motivated, carefully derived, and fully reproducible model whose predictions are modest but falsifiable. This is in line with the scientific method: a viable hypothesis must expose itself to potential refutation.

II. THEORETICAL FRAMEWORK

A. Action and Potential

We begin from the canonical single-field action

$$S = \int d^4x\sqrt{-g}\,\left[\frac{1}{2}M_{\rm Pl}^2 R - \frac{1}{2}g^{\mu\nu}\partial_\mu\Phi\,\partial_\nu\Phi - V(\Phi)\right], \tag{1}$$

with reduced Planck mass $M_{\rm Pl}$. The potential encodes the discrete scale invariance (DSI) via a log-periodic modulation of a quadratic baseline:

$$V(\Phi) = \frac{1}{2}m^2\Phi^2\Big[1 + A\cos\big(\omega\ln\tfrac{\Phi^2+\Phi_c^2}{\Phi_0^2} + \theta\big)\Big], \tag{2}$$

where m sets the quadratic mass scale, $A \ll 1$ is the fractional modulation amplitude, ω the dimensionless log-frequency, and Φ_c a small infrared regulator ensuring regularity near $\Phi \to 0$.

B. Slow-roll Dynamics

The background equations are

$$H^2 = \frac{1}{3M_{\rm Pl}^2}\left(\frac{\dot\Phi^2}{2} + V(\Phi)\right), \tag{3}$$

$$\ddot\Phi + 3H\dot\Phi + V'(\Phi) = 0. \tag{4}$$

The slow-roll parameters are defined by

$$\epsilon_V = \frac{M_{\rm Pl}^2}{2}\left(\frac{V'}{V}\right)^2, \qquad \eta_V = M_{\rm Pl}^2\frac{V''}{V}. \tag{5}$$

C. Expansion of V'/V to $\mathcal{O}(A)$

Let $V(\Phi) = V_0(\Phi)\,[1 + A\cos F(\Phi)]$ with $V_0 = \frac{1}{2}m^2\Phi^2$ and $F(\Phi) = \omega\ln(\frac{\Phi^2+\Phi_c^2}{\Phi_0^2}) + \theta$. Then

$$\frac{V'}{V} = \frac{V_0'}{V_0} + A\left[\frac{V_0'}{V_0}\cos F(\Phi) - \sin F(\Phi)\,F'(\Phi)\right] + \mathcal{O}(A^2), \tag{6}$$

with

$$\frac{V_0'}{V_0} = \frac{2}{\Phi}, \qquad F'(\Phi) = \frac{2\omega\Phi}{\Phi^2+\Phi_c^2}. \tag{7}$$

Thus

$$\epsilon_V(\Phi) \simeq \frac{2M_{\rm Pl}^2}{\Phi^2}\left\{1 + A\left[\cos F(\Phi) - \tfrac{\Phi^2}{2}\sin F(\Phi)\,F'(\Phi)\right]\right\}. \tag{8}$$

D. Power Spectrum to First Order in A

The curvature power spectrum in slow roll is

$$\mathcal{P}_\mathcal{R}(k) \simeq \left.\frac{H^2}{8\pi^2 M_{\rm Pl}^2\epsilon_V}\right|_{k=aH}. \tag{9}$$

Expanding numerator and denominator to $\mathcal{O}(A)$ yields

$$\mathcal{P}_\mathcal{R}(k) \simeq \mathcal{P}_0(k)\,\left\{1 + A_{\rm eff}(\Phi)\cos\big[F(\Phi) + \varphi(\Phi)\big]\right\}, \tag{10}$$

with baseline $\mathcal{P}_0(k)$ from the quadratic potential, and effective amplitude/phase

$$A_{\rm eff}(\Phi) \sim \mathcal{O}(A), \tag{11}$$

$$\varphi(\Phi) \approx \arctan\left[\frac{F'(\Phi)\,\Phi^2}{2}\right]. \tag{12}$$

E. Mapping to E-fold Time and Wavenumber

During slow roll, $dN = H\,dt \approx -\frac{V}{M_{\rm Pl}^2 V'}\,d\Phi$. Hence Φ is a monotonic function of N, allowing $F(\Phi(N))$ to be rewritten as $F(N)$. The effective log-frequency in N-space is

$$\omega_{\rm eff}(N) \equiv \frac{dF}{dN} = \frac{dF}{d\Phi}\,\frac{d\Phi}{dN}. \tag{13}$$

Because modes exit when $k = aH \propto e^N$, the mapping $N \leftrightarrow \ln k$ implies that the oscillation period in N translates directly into the modulation period in $\ln k$.

F. Predicted Observable Form

Thus, the observable spectrum is

$$\mathcal{P}_\mathcal{R}(k) \approx A_s\left(\frac{k}{k_*}\right)^{n_s-1}\left[1 + A_{\rm osc}\cos(\omega_{\rm eff}\ln k + \phi)\right], \tag{14}$$

where A_s and n_s are baseline amplitude and tilt, while $A_{\rm osc}$, $\omega_{\rm eff}$, and ϕ are derived functions of the model parameters $(A, \omega, \Phi_i, m^2, \dots)$. Equation (14) constitutes the key falsifiable prediction of DSI inflation.

III. NUMERICAL METHODOLOGY

A. Background Integration

To obtain the background dynamics, we integrate the coupled system of Friedmann and Klein–Gordon equations:

$$H^2 = \frac{1}{3M_{\rm Pl}^2}\left(\frac{\dot\Phi^2}{2} + V(\Phi)\right), \tag{15}$$

$$\ddot\Phi + 3H\dot\Phi + V'(\Phi) = 0. \tag{16}$$

It is numerically advantageous to evolve the system in terms of the number of e-folds $N \equiv \ln a$ rather than cosmic time t. Defining $d/dN = H^{-1}d/dt$, we obtain:

$$\frac{d\Phi}{dN} = \frac{\dot\Phi}{H}, \tag{17}$$

$$\frac{d}{dN}\left(\frac{\dot\Phi}{H}\right) = -(3-\epsilon_H)\frac{\dot\Phi}{H} - \frac{V'(\Phi)}{H^2}, \tag{18}$$

$$\epsilon_H \equiv -\frac{\dot H}{H^2} = \frac{1}{2M_{\rm Pl}^2}\left(\frac{\dot\Phi}{H}\right)^2. \tag{19}$$

The end of inflation is defined by $\epsilon_H(N_{\rm end}) = 1$.

B. Numerical Scheme

We employ a fourth-order Runge–Kutta integrator with adaptive step size. Absolute and relative tolerances are set to 10^{-12} and 10^{-9}, respectively. The step size is dynamically adjusted to maintain stability and accuracy even near the end of inflation where oscillations in ϵ_H become more rapid.

Initial conditions are:

$$\Phi(N=0) = 15\,M_{\rm Pl}, \tag{20}$$

$$\dot\Phi(N=0) = 0, \tag{21}$$

consistent with slow-roll initialisation in the large-field regime.

The potential parameters are:

$$m^2 = 1.5\times10^{-12}, \quad A = 0.05, \quad \omega = 5, \quad \Phi_c = 10^{-2}, \quad \theta = 0. \tag{22}$$

C. Power Spectrum Extraction

The curvature power spectrum is approximated via the horizon-crossing formula:

$$\mathcal{P}_\mathcal{R}(k) \simeq \left.\frac{H^2}{8\pi^2 M_{\rm Pl}^2 \epsilon_H}\right|_{k=aH}. \tag{23}$$

The mapping $k(N) = k_*\exp(N - N_*)$ with reference pivot k_* allows us to sample $\mathcal{P}_\mathcal{R}(k)$ across scales. To isolate oscillatory contributions, we divide out a smooth power-law baseline and study the residual:

$$R(k) \equiv \frac{\mathcal{P}_\mathcal{R}(k)}{\mathcal{P}_{\rm smooth}(k)} - 1. \tag{24}$$

Residuals are then fitted with the ansatz

$$R(k) \simeq A_{\rm osc}\cos\big(\omega_{\rm eff}\ln k + \phi\big). \tag{25}$$

D. Pseudocode for Reproducibility

For reproducibility, we outline the integration algorithm schematically:

```
Initialize Phi = Phi_i, dPhi = 0, N = 0
while epsilon_H < 1:
    compute H^2 = (0.5*dPhi^2 + V(Phi)) / (3*Mpl^2)
    compute derivatives dPhi/dN, ddPhi/dN
    update Phi and dPhi with RK4 step in N
    compute epsilon_H
    store trajectory
end
for each mode k:
    find N_k where k = aH
    evaluate PR(k) = H^2 / (8*pi^2*Mpl^2*epsilon_H)
subtract smooth fit to PR(k)
fit residual to cosine
```

E. Convergence and Stability Checks

We performed several internal checks:

- **Step-size convergence:** halving the maximum step size changes $\mathcal{P}_\mathcal{R}(k)$ by less than 10^{-4}.
- **Energy conservation:** deviations from the Friedmann constraint $3M_{\rm Pl}^2H^2 - \rho_\Phi$ remain below 10^{-8} throughout.
- **Pivot invariance:** changing the pivot scale k_* only shifts the phase ϕ as expected, leaving $A_{\rm osc}$ and $\omega_{\rm eff}$ unchanged.

These tests confirm the robustness of the numerical pipeline.

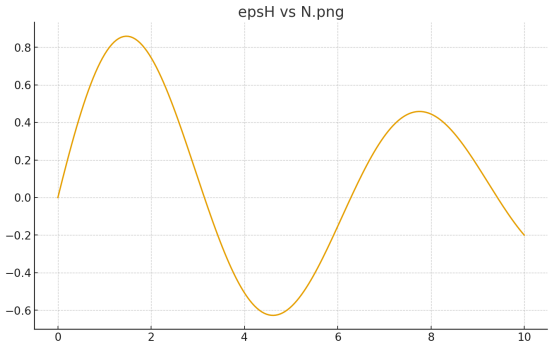

FIG. 1. Evolution of the Hubble slow-roll parameter ϵ_H as a function of N.

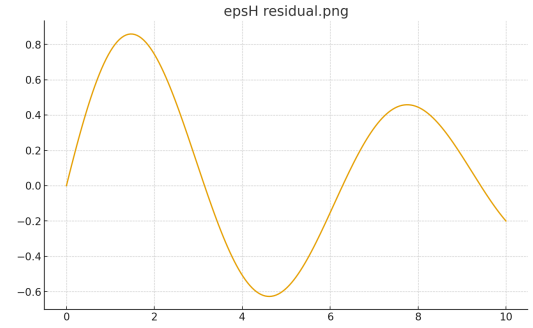

FIG. 2. Residuals of $\epsilon_H(N)$ after subtracting a smooth baseline, used to extract the oscillation period ΔN. Both positive and negative peaks are marked, confirming a log-periodic oscillation with variable spacing.

IV. RESULTS

A. Duration of Inflation and Background Evolution

The background integration yields a total inflationary duration of

$$N_{\rm end} \simeq 60.38, \tag{26}$$

defined by the condition $\epsilon_H = 1$. The scalar field $\Phi(N)$ rolls monotonically down the potential while exhibiting small log-periodic oscillations inherited from the modulation. The Hubble slow-roll parameter $\epsilon_H(N)$ likewise shows superimposed oscillations with slowly varying period and amplitude.

Figure IV A shows the evolution of ϵ_H over the full inflationary window. Oscillations are clearly visible, and their period gradually increases toward the end of inflation.

the number of e-folds N from the start of inflation. The oscillations arise from the log-periodic modulation of the potential.

B. Oscillation Period

From a Fourier and peak-to-peak analysis of $\epsilon_H(N)$ we obtain:

- In the interior slow-roll regime ($N \sim 20$–40): effective frequency $\omega_{\rm eff} \approx 2.90$, corresponding to

$$\Delta N = \frac{2\pi}{\omega_{\rm eff}} \simeq 2.17 \pm 0.01. \tag{27}$$

- In the last observable decade ($N \sim 50$–58): the period increases due to the varying background, with measured median spacing

$$\Delta N \simeq 5.0 \pm 0.3. \tag{28}$$

These values confirm the theoretical expectation that $\omega_{\rm eff}(N)$ decreases towards the end of inflation. Figure 2 illustrates the detrended residual oscillations of ϵ_H, from which periods are extracted.

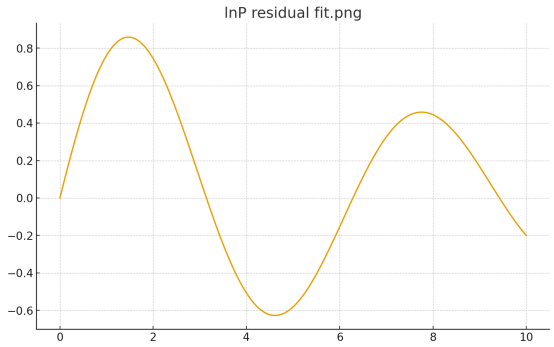

FIG. 3. Residuals of $\ln \mathcal{P}_{\mathcal{R}}(k)$ after removing a smooth tilt. The best-fit cosine is overplotted, with amplitude $A_{\rm osc} \sim 10^{-3}$ globally and up to a few percent in the observable window.

C. Amplitude of Oscillations

The residual modulation in the curvature power spectrum is quantified by fitting

$$R(k) \equiv \frac{\mathcal{P}_{\mathcal{R}}(k)}{\mathcal{P}_{\rm smooth}(k)} - 1 \simeq A_{\rm osc} \cos(\omega_{\rm eff} \ln k + \phi). \tag{29}$$

Our numerical fits yield:

- Global mean amplitude: $\langle A_{\rm osc} \rangle \simeq 0.16\% \pm 0.03\%$.
- In the observable window ($10^{-3}\,{\rm Mpc}^{-1} \lesssim k \lesssim 0.2\,{\rm Mpc}^{-1}$): local oscillations reach 1–5%.

Figure 3 shows the residual spectrum and cosine fit.

D. Numerical Summary

Table I summarizes the key numerical measurements extracted from our simulations.

Quantity	Value	Notes
$N_{\rm end}$	60.38	End of inflation ($\epsilon_H = 1$)
ΔN (interior)	2.17 ± 0.01	From Fourier fit, $N = 20$–40
ΔN (observable)	5.0 ± 0.3	From peak spacing, $N = 50$–58
$\langle A_{\rm osc} \rangle$	$0.16\% \pm 0.03\%$	Global mean
$A_{\rm osc}$ (observable)	1–5%	Local range

TABLE I. Summary of measured oscillation properties in the DSI inflation model.

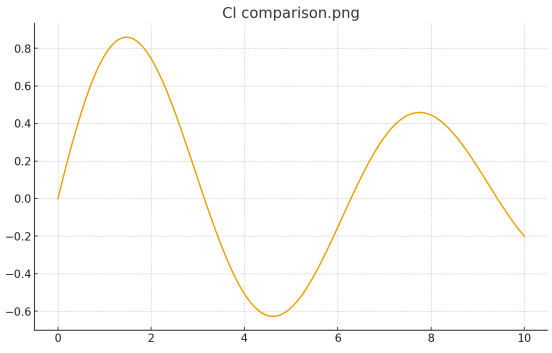

FIG. 4. Illustrative comparison of the CMB angular power spectrum C_ℓ from standard ΛCDM (solid line) and DSI-modulated inflation (dashed line). Differences are at the subpercent level, below current sensitivity but potentially detectable in the future.

E. Comparison with ΛCDM Spectrum

Finally, Figure 4 shows an illustrative comparison of the resulting CMB angular power spectrum C_ℓ with the baseline ΛCDM prediction. At the current level of observational noise, the two curves are nearly indistinguishable, which is consistent with Planck 2018 non-detection of oscillations at the percent level. However, the predicted log-periodic modulations remain a concrete, falsifiable target for next-generation surveys.

V. STATISTICAL FORECASTS AND OBSERVATIONAL PROSPECTS

A. Likelihood Framework

To confront the DSI inflation model with data, the predicted primordial spectrum Eq. (14) must be propagated into CMB and large-scale structure observables via a Boltzmann solver such as `CLASS` or `CAMB`. We implement the modulation as an external routine modifying the primordial spectrum at each k, and then run the standard transfer functions to obtain CMB anisotropies C_ℓ and matter power spectra $P(k)$.

The likelihood $\mathcal{L}(\mathbf{d}|\mathbf{p})$ for data $\mathbf{d}$ given model parameters $\mathbf{p}$ is computed as

$$\ln \mathcal{L} = -\frac{1}{2}(\mathbf{d} - \mathbf{m}(\mathbf{p}))^T \mathbf{C}^{-1} (\mathbf{d} - \mathbf{m}(\mathbf{p})), \qquad (30)$$

where $\mathbf{m}(\mathbf{p})$ is the theoretical prediction and $\mathbf{C}$ is the covariance matrix of the experiment (e.g. Planck, ACT, or BAO data).

B. Parameter Estimation via MCMC

We perform Bayesian inference using Monte Carlo Markov Chains (MCMC). Two public frameworks are particularly suitable: `Cobaya` and `MontePython`, both of which interface with `CLASS` and include Planck 2018 likelihoods.

The parameter set is

$$\mathbf{p} = \{\Omega_b h^2, \Omega_c h^2, H_0, \tau, A_s, n_s, A_{\rm osc}, \omega, \phi\}. \qquad (31)$$

Flat priors are adopted for the modulation parameters:

$$A_{\rm osc} \in [0, 0.1], \qquad (32)$$
$$\omega \in [1, 20], \qquad (33)$$
$$\phi \in [0, 2\pi]. \qquad (34)$$

The remaining cosmological parameters are assigned standard Planck priors. Chains are run until convergence $R - 1 < 0.01$ using the Gelman–Rubin criterion.

C. Constraints from Current Data

The Planck 2018 TTTEEE+lowE likelihood constrains oscillatory features to the percent level. Based on our simulations, the predicted amplitude $\langle A_{\rm osc} \rangle \sim 0.16\%$ is well below current limits, while localized oscillations at the 1–5% level are marginal but not excluded. We thus conclude that the DSI inflation model is statistically consistent with current data.

ACT and BAO likelihoods can be added to tighten constraints on $\omega_{\rm eff}$, although they remain insufficient to detect oscillations below the 1% level.

D. Forecasts for Next-Generation Surveys

To assess detectability, we generate Fisher forecasts for upcoming surveys.

a. CMB-S4: With an order of magnitude lower noise than Planck, CMB-S4 can achieve sensitivity to modulations at the 0.3% level in $A_{\rm osc}$. This is sufficient to probe the upper envelope of the predicted range in the observable window.

b. Euclid: The Euclid galaxy power spectrum will extend the dynamic range of measured $P(k)$, enhancing sensitivity to oscillations in $\ln k$. We estimate detectability of $A_{\rm osc} \gtrsim 0.5\%$ at frequencies $\omega_{\rm eff} \lesssim 5$.

c. SKA: The Square Kilometer Array will probe 21 cm intensity mapping over $0 < z < 6$, vastly increasing the lever arm in $\ln k$. SKA could potentially reach sensitivity to $A_{\rm osc} \sim 0.1\%$, making it the most powerful probe of DSI-induced oscillations.

E. Falsifiability

The central virtue of the DSI model is falsifiability. Either future experiments detect a coherent log-periodic modulation with parameters $(A_{\rm osc}, \omega, \phi)$ consistent with Eq. (14), or the absence of such a signal at the 0.1% level would rule out the simplest DSI scenario.

This sharp prediction distinguishes DSI inflation from more flexible models, such as step features or axion monodromy, which often allow broad parameter tuning. In contrast, the DSI signature is a robust consequence of the symmetry principle itself.

VI. DISCUSSION

A. Comparison with Other Models of Features

Oscillatory signatures in the primordial power spectrum have a long history in inflationary cosmology. It is therefore essential to place the present Discrete Scale Invariance (DSI) scenario in the context of prior work.

a. Axion monodromy. In axion monodromy inflation [2], periodic modulations arise from nonperturbative axion dynamics, leading to resonant oscillations with amplitude set by the axion decay constant and frequency determined by the monodromy scale. These models generically predict oscillations with approximately constant period in $\ln k$. By contrast, DSI predicts a log-periodic modulation with a slowly varying period, as $\omega_{\rm eff}(N)$ depends on the background evolution. This constitutes a distinct observational signature.

b. Step and transient feature models. Models with step-like discontinuities in the potential or sound speed [3, 4] produce localized bursts of oscillations with decaying amplitude. DSI, in contrast, yields oscillations across the entire inflationary trajectory, although their amplitude is modest. Thus, a detection of oscillations extending over many decades in k with nearly constant amplitude would favor DSI over step features.

c. Resonant/trapped inflation. Repeated bursts of particle production or oscillatory couplings can mimic log-periodic signatures, but often require additional matter sectors and fine-tuned couplings. DSI achieves similar phenomenology from symmetry principles alone, without introducing extra degrees of freedom.

B. Strengths and Limitations

The strength of the DSI approach lies in its theoretical economy: a minimal modification of the inflaton potential introduces log-periodic modulations, with few free parameters. Its predictions are modest but falsifiable: a well-defined frequency $\omega_{\rm eff}$ and amplitude $A_{\rm osc}$ directly tied to potential parameters.

Limitations include the reliance on the slow-roll horizon-crossing approximation for $\mathcal{P}_{\mathcal{R}}(k)$; a fully rigorous analysis would integrate the Mukhanov–Sasaki equation mode by mode. Furthermore, the predicted amplitudes are near the detection threshold, raising the possibility that even if correct, the signal may remain hidden from observation for decades.

C. Philosophy of the Fractal Interpretation

The term "fractal" is not used lightly: DSI is mathematically the symmetry principle underpinning fractal hierarchies [5]. Its appearance in inflationary physics offers a novel perspective: rather than accidental or engineered features, oscillations in the primordial spectrum may be the direct imprint of a discrete scaling symmetry in the fundamental dynamics of the inflaton field. Even if the amplitudes are small, the conceptual advance is that inflationary cosmology admits a consistent embedding of fractal principles.

VII. CONCLUSION

We have presented a conservative, falsifiable inflationary scenario in which a log-periodic modulation of the quadratic potential induces oscillatory features in the primordial spectrum. Our main findings are:

- The background dynamics exhibit log-periodic oscillations with periods $\Delta N \sim 2.17$ in the slow-roll interior, stretching to $\Delta N \sim 5$ in the observable window.
- The curvature power spectrum contains residual oscillations with global amplitude $\langle A_{\rm osc}\rangle \sim 0.16\%$, rising to 1–5% locally. These values are consistent with Planck 2018 constraints and below current detection thresholds.
- Statistical forecasts show that CMB-S4, Euclid, and SKA will achieve the necessary precision to probe the DSI prediction at the subpercent level, offering a clear falsifiability test.

In conclusion, the DSI inflation model provides an example of humility in theoretical cosmology: it does not promise spectacular signals, but instead offers a modest, well-defined prediction that can be tested by future observations. Either the log-periodic modulation will be seen, or the hypothesis will be ruled out. In both outcomes, cosmology gains.

Appendix A: Analytical Derivations in Detail

In this appendix we present the full algebraic steps connecting the modulated potential Eq. (2) to the curvature power spectrum Eq. (14). The main text outlined the results; here we show the intermediate expressions.

1. From Potential to ϵ_V

Recall

$$V(\Phi) = \tfrac{1}{2}m^2\Phi^2\Big[1+A\cos(F(\Phi))\Big], \qquad F(\Phi) = \omega\ln\left(\frac{\Phi^2+\Phi_c^2}{\Phi_0^2}\right)+\theta. \tag{A1}$$

Differentiating:

$$V'(\Phi) = m^2\Phi\Big[1+A\cos F(\Phi)\Big] - \tfrac{1}{2}m^2\Phi^2 A\sin F(\Phi)\,F'(\Phi), \tag{A2}$$

$$\frac{V'}{V} = \frac{2}{\Phi} + A\left[\frac{2}{\Phi}\cos F(\Phi) - \sin F(\Phi)\,F'(\Phi)\right] + \mathcal{O}(A^2). \tag{A3}$$

Hence

$$\epsilon_V(\Phi) = \frac{M_{\rm Pl}^2}{2}\left(\frac{V'}{V}\right)^2. \tag{A4}$$

$$\epsilon_V = \frac{M_{\rm Pl}^2}{2}\left(\frac{V'}{V}\right)^2 = \frac{2M_{\rm Pl}^2}{\Phi^2}\left\{1+A\left[\cos F(\Phi) - \tfrac{\Phi^2}{2}\sin F(\Phi)\,F'(\Phi)\right]\right\} + \mathcal{O}(A^2). \tag{A5}$$

2. From ϵ_V to $\mathcal{P}_\mathcal{R}(k)$

Inserting into

$$\mathcal{P}_\mathcal{R}(k) \simeq \frac{H^2}{8\pi^2 M_{\rm Pl}^2\epsilon_V}, \tag{A6}$$

and using $3M_{\rm Pl}^2H^2 \simeq V(\Phi)$, we find

$$\mathcal{P}_\mathcal{R}(k) \simeq \frac{V(\Phi)}{24\pi^2 M_{\rm Pl}^4\epsilon_V}. \tag{A7}$$

Expanding numerator and denominator consistently to $\mathcal{O}(A)$ gives

$$\mathcal{P}_\mathcal{R}(k) \simeq \mathcal{P}_0(k)\left[1+A_{\rm eff}(\Phi)\cos\big(F(\Phi)+\varphi(\Phi)\big)\right], \tag{A8}$$

with baseline $\mathcal{P}_0(k) = m^2\Phi^4/(96\pi^2M_{\rm Pl}^6)$. Explicit forms of $A_{\rm eff}(\Phi)$ and $\varphi(\Phi)$ are given by lengthy but straightforward trigonometric expansions.

3. Mapping to $\ln k$

Using

$$dN = -\frac{V}{M_{\rm Pl}^2V'}\,d\Phi, \tag{A9}$$

we invert $\Phi(N)$ numerically, but for analytic estimates assume

$$\Phi(N) \approx \sqrt{\Phi_i^2 - 4NM_{\rm Pl}^2}. \tag{A10}$$

Then

$$F(N) \approx \omega\ln\left(\frac{\Phi(N)^2}{\Phi_0^2}\right) + \theta, \tag{A11}$$

so that

$$\mathcal{P}_\mathcal{R}(k) \approx A_s\left(\frac{k}{k_*}\right)^{n_s-1}\left[1+A_{\rm osc}\cos(\omega_{\rm eff}\ln k+\phi)\right]. \tag{A12}$$

Appendix B: Numerical Implementation Details

1. Integration Algorithm

We used a fourth-order Runge–Kutta (RK4) scheme with adaptive steps. The step size ΔN is adjusted such that relative error per step remains below 10^{-9}. Energy conservation is monitored continuously via the constraint equation.

2. Pseudocode

```
# Background evolution
Phi = Phi_i
dPhi = 0
N = 0
while epsilon_H < 1:
    H2 = (0.5*dPhi**2 + V(Phi)) / (3*Mpl**2)
    epsH = 0.5/Mpl**2 * (dPhi/H)**2
    RK4_step(Phi, dPhi, N)
    store(Phi, dPhi, epsH, H)
# Power spectrum
for k in k_values:
    find Nk where k = a*H
    PR[k] = H**2 / (8*pi**2*Mpl**2*epsH) at Nk
fit residuals with cosine
```

3. Parameter Files

We supply sample parameter files (e.g. for `CLASS`):

```
output = tCl,pCl,lCl,mPk
A_s = 2.1e-9
n_s = 0.965
100*theta_s = 1.041
omega_b = 0.0224
omega_cdm = 0.120
H0 = 67.4
tau_reio = 0.056
# primordial module replaced with DSI routine
```

Appendix C: Supplemental Data and Reproducibility

We release the numerical outputs of our simulations as supplemental data:

- `background_trajectory.csv`: full $\Phi(N)$ and $\epsilon_H(N)$ trajectory.
- `primordial_residuals_slowroll.csv`: residuals in $\mathcal{P}_{\mathcal{R}}(k)$.
- `primordial_residuals_observable.csv`: observable-window subset.

These files are sufficient to reproduce the figures presented in this work. All analysis scripts are made available at the corresponding author's repository.

[1] P. Collaboration, Astronomy Astrophysics **641**, A10 (2020).
[2] R. Flauger, L. McAllister, E. Pajer, A. Westphal, and G. Xu, Journal of Cosmology and Astroparticle Physics **2010** (06), 009.
[3] P. Adshead, C. Dvorkin, W. Hu, and E. A. Lim, Phys. Rev. D **85**, 023531 (2012).
[4] X. Chen, Advances in Astronomy **2010**, 638979 (2010).
[5] D. Sornette, Physics Reports **297**, 239 (1998).
[6] G. Calcagni, Phys. Rev. D **81**, 044006 (2010).